



Effects of SNR-Dependent Beam Alignment Errors on Millimeter-Wave Cellular Networks

Muhammad Saad Zia , *Student Member, IEEE*, Douglas M. Blough , *Senior Member, IEEE*,
and Mary Ann Weitnauer, *Senior Member, IEEE*

Abstract—At millimeter-wave (mm-wave) frequencies, narrow beamwidth and inaccurate channel estimation result in beam alignment errors, which degrade the achievable signal-to-noise ratio (SNR) and rate. The extent of beam misalignment depends on the various link parameters, however, prior works ignored such a dependence and considered oversimplified array patterns. This paper formulates beam alignment errors for the uniform linear array at the base station as a function of the link parameters by using the Cramér Rao lower bound of angle-of-arrival estimates and proposes a tractable array pattern approximation to better reflect the effects of such alignment errors. Utilizing stochastic geometry and the statistics of the Student's t -distribution, a novel and robust analytical technique is developed to obtain the downlink SNR and rate coverage probabilities due to beam misalignment, assuming a single antenna at the user. We show that beam alignment errors significantly affect the achievable SNR and rate for non line-of-sight (NLOS)/distant users whereas the effect is negligible for LOS/nearby users. It is also illustrated that the effects of alignment errors cannot be mitigated only by increasing the number of antennas. We also show that our proposed array pattern approximation better captures the effects of beam alignment errors as compared to the widely used flat-top pattern.

Index Terms—Array pattern, beam alignment error, Cramér Rao lower bound, element pattern, Student's t -distribution.

I. INTRODUCTION

THE sub-6 GHz band, which is traditionally used for cellular communications, has become extremely crowded and is unable to cope with the accelerating demand for higher data rates [1], [2]. The millimeter-wave (mm-wave) frequency band (30–300 GHz), on the other hand, is currently under-utilized and offers large swaths of contiguous bandwidth [3]; thus, it is seen as a promising solution for beyond 5G (B5G) systems [4]. Nevertheless, the mm-wave frequencies have inherent challenges, which are distinct from their sub-6 GHz counterparts. A pressing challenge is the higher path loss [5].

The use of antenna arrays, consisting of a large number of antenna elements, allows to compensate for the signal attenuation due to the increased path loss. Increasing the number of

antenna elements makes the transmissions highly directional by rendering the main lobe narrow and enhancing its power gain [6]. This feature also reduces the interference in the network and the mm-wave systems tend to be noise-limited with a moderate base station (BS) deployment [7]. Because of the directional transmissions, mm-wave channels are sparse and this sparsity causes enhanced sensitivity to blockages in the environment [5]. Blockages are a major concern in mm-wave systems as they result in different path loss characteristics for the line-of-sight (LOS) and non-LOS (NLOS) propagation [8].

Fully digital beamforming is not considered a feasible approach at mm-wave frequencies because of practical limitations [9]. Therefore, analog beamforming has been proposed in which a network of phase-shifters is used to spatially steer the beam towards the dominant propagation path [10]. Though analog beamforming supports only a single beam, it is generally regarded as an immediate solution for mm-wave cellular systems as it has already been adopted in the IEEE 802.11ad standard. To configure the beamforming coefficients, the angle-of-departure (AoD)/angle-of-arrival (AoA) corresponding to the dominant propagation path is required. Such information can either be obtained through the use of beam training approaches or by directly estimating the channel [10]–[14]. The beam training approaches iteratively select the beamforming vectors from predefined codebooks to maximize the link signal-to-noise ratio (SNR) [12]. To realize higher beamforming gains, direct estimation of the channel is necessary, albeit it is extremely challenging at mm-wave frequencies because of the large number of antennas involved and the low SNR before beamforming [11]. Channel estimation schemes for massive multiple-input multiple-output (MIMO) systems were proposed in [13], [14]. In [15], a practical and low complexity channel estimation scheme was proposed for beam alignment in mm-wave systems. The method of [15] utilized sparse bipartite graphs to estimate the beamforming direction from compressive phaseless measurements.

Irrespective of how the beamforming coefficients are configured, perfect beam alignment is hard to realize in mm-wave systems because of the errors in AoA/AoD estimation [16], [17]. The misalignment results in a suboptimal array gain, which reduces the SNR and the rate on the desired link. Therefore, it is important to analyze the effect of beam misalignment on the system level performance of mm-wave networks.

This paper investigates the impacts of beam alignment errors, arising from imperfect channel estimation, on the system-level downlink achievable SNR and rate of a mm-wave cellular

Manuscript received August 31, 2021; revised January 1, 2022; accepted February 9, 2022. Date of publication March 1, 2022; date of current version May 20, 2022. The review of this article was coordinated by Prof. Hsiao-Feng Lu. (*Corresponding author: Muhammad Saad Zia.*)

The authors are with the School of Electrical and Computer Engineering, Georgia Institute of Technology, Atlanta, GA 30332-0765 USA (e-mail: saad.zia@gatech.edu; doug.blough@ece.gatech.edu; mary.ann.weitnauer@ece.gatech.edu).

Digital Object Identifier 10.1109/TVT.2022.3155386

network. We formulate the alignment error model using the Cramér-Rao lower bound (CRLB) of AoA estimates. Based on this formulation, we devise analytical approaches to obtain the SNR coverage and rate coverage results. Using simulations for the CRLB model, we then verify our analytical results. For the SNR coverage, we also simulate the beam alignment scheme of [15] and show that it provides similar findings as our proposed CRLB-based approach. The beam alignment error in all the above approaches takes into account the effects of path loss, blockage, directional antenna elements and the array factor. The rate analysis takes into account the loading on the BSs.

A. Related Work

In the following, we discuss the related work and highlight the limitations of the existing research. We start by giving a brief overview of some of the commonly employed array pattern approximations and then review the available literature relevant to beam alignment errors.

Owing to its mathematical tractability, stochastic geometry has recently been extensively employed for detailed system-level performance evaluations of cellular networks [18]. Additionally, because of the highly directional transmissions, the effect of different array pattern approximations on the system-level performance of mm-wave networks has also been investigated in many works (e.g., [6]).

Most of the existing works on mm-wave networks adopt the flat-top pattern for simplicity of analysis, however, such a pattern fails to model the inherent gradual roll-off of a realistic array pattern. With the flat-top pattern, the array gain is characterized by only two constant gain values [10]. Within the half-power beamwidth (HPBW), the array gain equals the peak main lobe gain, while it equals the maximum of the first side lobe outside the HPBW [6]. Moreover, the HPBW, the peak main-lobe gain and the side lobe level (SLL) of an array pattern all depend on the number of antenna elements. However, in [2], [7], [8], such a dependence was ignored while using the flat-top pattern. In [16], an enhanced flat-top pattern was proposed in which the HPBW and the SLL scaled with the number of elements, but the maximum array gain was normalized to 1 for analytical tractability.

Motivated by the limitations of the flat-top pattern, the sinc pattern and a cosine pattern approximation were proposed in [6] for a uniform linear array (ULA). It was shown in [6] that increasing the number of antenna elements in the array increases the coverage probability for mm-wave *ad-hoc* and cellular networks. The effects of beam alignment errors were, however, ignored in the analysis.

The issue of beam misalignment in mm-wave communications has been studied in several existing research works. Adopting beam training approaches for beam alignment, [19] derived analytical bounds for the probability of beam misalignment considering a single-path mm-wave channel. Moreover, the probability of misalignment was found to decrease as the length of the training pilot sequence increased. A performance comparison was also done for the two most common beam training approaches, i.e., exhaustive search and hierarchical search,

where it was observed that beam alignment through exhaustive search leads to a lower probability of misalignment and a higher spectral efficiency as compared to hierarchical search for a fixed training overhead.

The design of a hierarchical beam training codebook was studied in [20] with the aim of reducing the beam alignment errors. Specifically, new training beams were designed by shaping the geometric beam patterns and a new structure of the codebook was devised to minimize the alignment errors. A codebook design was also proposed in [21] to minimize the beam alignment errors. Based on a Markov decision process (MDP) formulation, an energy-efficient beam alignment protocol was proposed in [22], where the relation between the energy consumed during beam alignment and the corresponding alignment errors was investigated considering the flat-top pattern. For a certain probability of the beam alignment error, it was observed that achieving higher spectral efficiency required more energy consumption. It is worth mentioning here that the system models of [19]–[22] considered beam training approaches and were limited to a single BS and a single user.

The works in [23], [24] considered beam alignment errors arising due to imperfect mm-wave channel estimation. With a goal to alleviate the performance loss due to beam misalignment in a single user system, [23] proposed a beam misalignment aware transceiver design that incorporated the statistics of the beam alignment errors, which followed a uniform distribution. Along similar lines, a multi-user precoding design was proposed in [24], where the beam alignment errors for all the users followed the same uniform distribution.

Though the above works [19]–[24] addressed beam alignment errors, they focused on a single BS system model and ignored system-level aspects such as the random path-loss and blockage statistics. Hence, these works did not provide any insights on the holistic network performance. Below, we overview some of the works that have evaluated the effects of beam alignment errors on the system-level performance of mm-wave networks.

The effects of beam misalignment on a mm-wave *ad-hoc* network were studied in [25] using the flat-top pattern and a Gaussian pattern. While the Gaussian pattern consists of a gradual roll-off, its parameters in [25] were chosen arbitrarily without any consideration of the array characteristics. Using stochastic geometry, it was shown that even small alignment errors cause significant loss in ergodic capacity, which the flat-top pattern fails to capture. A study using the cosine array pattern in a device-to-device (D2D) mm-wave network showed that beam alignment errors can degrade the coverage by up to 35% [17]. Using the flat-top pattern, it was shown in [18] that the degradation in the coverage and average rate of a mm-wave cellular network is considerable when the standard deviation of the alignment error is greater than 6° . For a three tier mm-wave heterogeneous cellular network, however, it was observed in [26] that the deterioration in coverage becomes evident when the standard deviation exceeds 7° . Using the enhanced flat-top antenna model, the authors in [16] observed that increasing the number of antenna elements increases the coverage for small beam alignment errors, however, doing so in the presence of large alignment errors decreases the coverage severely.

While [16]–[18], [25], [26] used a truncated Gaussian distribution to model the beam alignment errors, the dependence of such errors on the underlying system parameters was not established. The coverage and rate results were compared for different values of the standard deviation of the alignment error without specifying how the standard deviation is obtained. To the best of our knowledge, besides our earlier work [27], no other work has tried to address this. In [27], the authors formulate the standard deviation of the alignment error as a function of the SNR of the pilot signal used for channel estimation. A tractable array pattern approximation, which consists of a gradual roll-off and follows the 3GPP model of [28], is also proposed in [27] to analyze the effects of beam misalignment on the downlink SNR coverage probability.

B. Contributions

Below, we state our contributions and underline the novelty of this paper. Different from our prior work [27], in this paper we propose a more analytically robust approach to obtain the downlink SNR coverage probability and we extend to the rate coverage analysis. Also different from [27], we illustrate how the flat-top pattern compares with the proposed 3GPP pattern approximation when the SNR dependence of beam alignment errors is incorporated. The main contributions of this paper are summarized as follows.

- *We apply the Cramér-Rao lower bound (CRLB) to capture the dependence on the link parameters.* By using the CRLB of AoA estimates, we formulate the statistics of the downlink beam alignment errors in terms of the link state, the path-loss and the antenna array configuration. Prior works (e.g., [16], [17]) chose a fixed variance without consideration for how the link parameters affect the alignment error.
- *We adopt the 3GPP array pattern approximation and compare the results with the flat-top pattern.* For beam alignment error analysis, most prior works (e.g., [16], [18]) use the flat-top pattern, which offers no penalty in terms of the array gain for small values of the alignment error and extreme penalty for large alignment errors. By comparison with our 3GPP pattern approximation, we illustrate that the flat-top pattern underestimates the SNR and rate for distant/NLOS user equipments (UEs) and overestimates the same for near/LOS UEs.
- *We obtain tractable expressions for the downlink SNR coverage with imperfect beam alignment.* Different from our previous work in [27], we utilize the statistics of the Student's t -distribution to capture the effects of the directional element pattern and the path-loss. Our results show that increasing the BS density and the array size provide varying benefits in the presence of beam alignment errors.
- *We analyze the rate coverage with imperfect beam alignment.* Whereas the SNR coverage is representative of the quality of the links, the rate coverage is illustrative of the achievable network throughput as it takes the load into account. We show that the benefits obtained from increasing the BS density and the array size follow a different pattern from the SNR coverage.

C. Organization of the Paper

The rest of this paper is organized as follows. Section II explains the system model. Analytical formulation of the downlink SNR coverage probability is given in Section III while Section IV presents the downlink rate coverage probability. The results are discussed in Section V. Finally, Section VI concludes the paper.

II. SYSTEM MODEL

In this section, we introduce our system model for the downlink beam alignment error analysis of a mm-wave cellular network. We also propose a tractable array pattern approximation for a ULA and characterize the beam alignment errors in terms of the link parameters in the following.

A. BS and User Locations

The BS locations are modeled in \mathbb{R}^2 as a homogeneous Poisson point process (PPP) Φ_B of intensity λ_B . All the BSs transmit at a constant power level P_d . The user locations are modeled as an independent homogeneous PPP Φ_u with intensity λ_u . According to Slivnyak's theorem and as per the standard practice in stochastic geometric analysis, a *typical user* is assumed to be located at the origin and the analysis is performed on this typical user [29]. The BS serving the typical user is termed as the *tagged BS*.

B. Beamforming Model

To compensate for the high path-loss and to provide an acceptable link quality, mm-wave systems require beamforming using antenna arrays [30], [31]. Traditional wireless systems operating at lower frequencies commonly employ digital beamforming, which requires a dedicated radio frequency (RF) chain for each antenna element as all the processing is done in the baseband [9]. However, the high cost and power consumption of the RF chains and mixed-signal components, e.g., digital-to-analog converters (DACs) at mm-wave frequencies, and the use of large number of antenna elements render digital beamforming impractical in mm-wave systems [4], [31], [32]. Because of the above-mentioned hardware limitations, analog beamforming is widely considered as a practical solution for mm-wave cellular systems as its implementation complexity is low and it has already been standardized for other systems operating on mm-wave frequencies, such as IEEE 802.11ad [4], [33].

In this paper, similar to [6], [10], [34], we consider that each BS employs analog beamforming in which all the antenna elements of a BS's array are connected to a single RF chain via a network of phase-shifters, as shown in Fig. 1. Each UE is assumed to have a single isotropic antenna [6], [35]. With such a beamforming model, a BS forms a single communication beam that can be spatially steered to serve a user by adjusting the weights of the phase-shifters [33].

It is worth mentioning here that to serve multiple users simultaneously (i.e., multi-user transmission) by forming multiple simultaneous beams, the existing literature on mm-wave systems proposes a hybrid beamforming architecture, where a large number of antenna elements are connected to a small

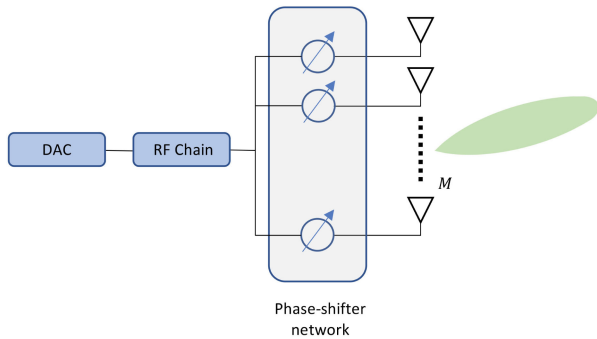


Fig. 1. Analog beamforming architecture at the BS. An array of M antenna elements is connected to a single RF chain via a network of phase-shifters, and forms a single communication beam.

number of RF chains and the number of beams is bounded by the number of RF chains [9], [30], [33]. Multi-user interference is an important aspect of multi-user transmission. In this work, we do not consider hybrid beamforming and, therefore, defer multi-user transmission for future work.

With analog beamforming, however, each BS uses a scheduler to serve its associated users using single stream transmission. We assume that the users are scheduled in a round robin manner [10]. To serve a scheduled user, the serving BS steers its beam towards the dominant propagation path for that user in order to maximize the received signal power [10], [33]. If the tagged BS, located at x , transmits a symbol s_0 with an array of M antenna elements using analog beamforming towards the typical user, then the received signal at the typical user is given as

$$u_0 = \sqrt{P_d L_k(r) \tilde{G}_A(\phi, \theta) \varrho_k} s_0 + \text{OCI} + n_0, \quad (1)$$

where P_d is the BS transmit power, $L_k(r)$ is the path-loss at a distance $r = \|x\|$ with link state k , $\tilde{G}_A(\phi, \theta)$ is the antenna array pattern, ϱ_k is the small-scale fading coefficient for link state k , and n_0 is the additive white Gaussian noise with power σ_n^2 . The term OCI represents the out-of-cell interference, which is caused by other BSs. The values of the BS density, λ_B , used in this work correspond to a noise-limited network [7], [9], where out-of-cell interference is negligible. Therefore, we do not characterize the OCI. The terms $L_k(r)$, ϱ_k and $\tilde{G}_A(\phi, \theta)$ are described in more detail in the following subsections.

C. Link State, Path-loss and User Association Models

We model the mm-wave propagation using the two-state statistical link model wherein a link can either be in a LOS state or a NLOS state and the path-loss for the two states is defined separately [1], [2]. For simplicity of notation, the LOS and NLOS channel states are denoted as ‘‘L’’ and ‘‘N’’ respectively. Some works, such as [18], also consider an *outage* state, in which the path-loss is assumed to be infinite. However, ignoring the outage state does not compromise the accuracy of the analysis [36]. If the length of a link is r and the link belongs to the k^{th} channel state for $k \in \{L, N\}$, then the path-loss for the link is expressed as

$$L_k(r) = C_k r^{-\alpha_k}, \quad (2)$$

where C_k and α_k are obtained from the empirically observed data. We adopt the *floating-intercept* model according to which α_k is the slope of the best linear fit to the empirical data and C_k is the corresponding floating intercept [3]. We further assume that each UE gets associated to the BS that offers the minimum path loss, i.e., the maximum average received power. The effects of beam alignment errors are ignored while deciding the associations [18].

D. Blockage Model

The sensitivity to blockages is a key distinguishing feature of mm-wave propagation. The link state probabilities depend on the statistics of blockages/obstacles in a certain area and the link distance. To establish such probabilities, different statistical blockage models have been proposed in the literature [10]. This paper adopts the generalized LOS ball blockage model, which approximates the LOS region around a BS/user by a ball of a specific fixed radius R_B [2]. Inside the ball, a link can either be LOS or NLOS. Outside the ball, every link is NLOS. With such a model, the probability for a link to be LOS is expressed in [37] as $\mathcal{P}_L(r) = \mu \cdot \mathbb{1}(r < R_B)$, where μ represents the *average LOS fractional area* in the network, $\mathbb{1}(\cdot)$ is the indicator function and R_B represents the maximum range of a LOS link. The values of R_B and \mathcal{P}_L depend on the geographic area in which the network is deployed and are obtained empirically. The LOS ball model is an analytical approximation with a relatively simple form, yet it provides SINR statistics that match very well with the SINR obtained in the presence of actual blockages [10].

E. Fading Model

A clustered channel model, where each cluster corresponds to a macro-level scattering path, has been shown to match empirical data well for mm-wave propagation [5]. The number of clusters is small in mm-wave channels because of the high path-loss experienced by the excess-delayed paths [38]. The small-scale fading effects in such a model are captured by considering that each cluster is a summation of multiple sub-paths.

The channel coefficients of the different sub-paths within a cluster are usually modeled analytically as independent and identically distributed complex Gaussian RVs with zero mean and some variance, which corresponds to the average cluster energy [39]. However, as shown in [40], the fading envelope due to the combined effect of such channel coefficients can be equivalently represented in the form of a single Nakagami random variable (RV). The small-scale fading effects in a cluster can, thus, be emulated by considering a single sub-path with Nakagami fading, as in [6].

Due to its versatility, the Nakagami distribution allows to model different levels of small-scale scattering just by varying the Nakagami shape parameter. As a result, to distinguish the small-scale effects for LOS and NLOS propagation, we use different Nakagami shape parameters, N_L and N_N , where both are integers and $N_L > N_N$ since a small value of the shape parameter means a larger scattering variance [8]. Let ϑ_k represent the Nakagami channel coefficient for $k \in \{L, N\}$. The corresponding channel gain, $\varrho_k = |\vartheta_k|^2$, then becomes a *normalized* gamma RV whose probability density function (PDF)

is expressed as [16]

$$f_{\varrho_k}(z; N_k, N_k) = \frac{N_k^{N_k} z^{N_k-1} \exp(-N_k z)}{\Gamma(N_k)}. \quad (3)$$

Considering analog beamforming with single stream transmission at the BS, the downlink received signal power at the desired UE is maximized by steering the main lobe of the BS's array pattern towards the dominant channel cluster for that UE [36]. The beamforming vector in such a case is parameterized by a single angle that corresponds to the strongest path direction [32]. Such an approach results in an optimal beamforming gain for the system under consideration [41].

Because of the above-mentioned justifications and to enable analytical tractability, we only consider the dominant cluster and model the mm-wave channel as a single cluster and single sub-path channel with independent Nakagami fading for each link.

The single-cluster single-path channel model has been adopted in many other analytical works (e.g., [6], [42] and [32]) for mm-wave network performance analysis using stochastic geometry, though with an omnidirectional antenna element pattern. Moreover, in [42], it was shown using simulations that a mm-wave channel with 3 clusters provides similar insights (with slight scaling differences) as the single-cluster single-path channel model.

F. Antenna Array Pattern and Channel Model

In this subsection, we define two channel models. First, we describe a reference channel model based on the vector channel from the BS array to the UE antenna. Second, we describe the effective scalar channel model that we use, which incorporates the 3GPP array pattern approximation to facilitate the network performance analysis.

This paper considers antenna arrays only at the BSs whereas a single isotropic antenna is assumed at each UE [35]. We further assume that the arrays at the BSs are composed of directional antenna elements as they offer higher directivity and increased sidelobe attenuation as compared to omnidirectional elements [36]. Moreover, we assume that each BS utilizes three sectors to provide coverage and each sector is equipped with a ULA comprising M directional antenna elements. We consider beamsteering capability along the azimuth plane only while the elevation angle is kept fixed at $\frac{\pi}{2}$ [36]. The field of view of a sector is, therefore, $[-\frac{\pi}{3}, \frac{\pi}{3}]$ in the horizontal plane.

For our reference channel model, we consider the array response pattern, $G_A(\phi, \theta)$, as

$$G_A(\phi, \theta) = G_e(\phi) \cdot \text{AF}(\phi, \theta), \quad (4)$$

where $G_e(\cdot)$ represents the gain due to the element pattern, $\phi \in [-\frac{\pi}{3}, \frac{\pi}{3}]$ is the true direction of the dominant propagation path with respect to the boresight of the array and $\theta \in [-\frac{\pi}{3}, \frac{\pi}{3}]$ represents the mainlobe steering direction. It is important to mention here that θ is an estimate of ϕ and is, therefore, affected by beam alignment errors. In the absence of such errors, θ equals ϕ . In (4), the subscripts e and A stand for the single element and array, respectively. The term $\text{AF}(\phi, \theta)$ is the gain due to the array factor, which depends on the number of antenna

elements and the physical array configuration. The array factor gain is represented as $\text{AF}(\phi, \theta) = |\mathbf{w}^H(\phi) \cdot \mathbf{a}(\theta)|^2$, where H is the Hermitian operator, $\mathbf{a} \in \mathbb{C}^M$ is the vector of beamforming weights and $\mathbf{w} \in \mathbb{C}^M$ is the channel response vector, which depends on the angle ϕ . For a ULA, the channel response vector for a single path channel is given by

$$\mathbf{w}(\phi) = \left[1, e^{j\frac{2\pi d}{\lambda_c} \sin(\phi)}, \dots, e^{j\frac{2\pi(M-1)d}{\lambda_c} \sin(\phi)} \right]^T, \quad (5)$$

where d is the spacing between adjacent antenna elements, which is kept at half-wavelength, and λ_c is the carrier wavelength. With analog beamforming, the BS spatially steers its transmit beam to the desired angle. The beamforming vector $\mathbf{a}(\theta)$, in this case, is the spatial matched filter corresponding to a path at angle θ and is expressed the same way as $\mathbf{w}(\phi)$ but scaled by $1/\sqrt{M}$ and with ϕ replaced by θ .

To define the element pattern in our model, we use the 3GPP specifications [43]. The power, in dB, radiated by a single directional element in a direction ϕ is then written as

$$G_e^{(dB)}(\phi) = G_{\max} - \min \left[12 \left(\frac{\phi}{\varphi_e} \right)^2, A_m \right], \quad (6)$$

where $G_{\max} = 8$ dBi is the maximum gain of the single element, $A_m = 30$ dB is the front-to-back ratio, and $\varphi_e = 65^\circ$ is the half-power beamwidth (HPBW) of the element.

Thus, a single-cluster and single-path channel model, including fading and path-loss, may be expressed as $\sqrt{L_k(r)} \varrho_k \mathbf{w}^H(\phi)$. The BS beamforming weights and antenna element pattern may be incorporated to define a reference scalar channel model to be from the BS beamport to the UE antenna port, in which case the reference channel model becomes $\sqrt{L_k(r)} G_A(\phi, \theta) \varrho_k$.

However, network performance analysis using the array pattern of (4) is extremely challenging [6]. To facilitate the analysis, the array pattern of a ULA is approximated in this paper using the 3GPP antenna gain pattern mentioned in [28]. The 3GPP array pattern approximation consists of a main lobe with a gradual roll-off and an average SLL. The gradual roll-off becomes important when analyzing the impact of beam misalignment. The approximated array radiation pattern, $\tilde{G}_A(\phi, \theta)$ can be written as [28]

$$\tilde{G}_A(\phi, \theta) = \begin{cases} G_1(\phi) 10^{\frac{-3}{10} \left(\frac{2(\phi-\theta)}{\varphi_A} \right)^2} & \text{if } |\phi - \theta| \leq \Theta_A \\ G_2 & \text{if } \Theta_A \leq |\phi - \theta| \leq \pi, \end{cases} \quad (7)$$

where $\varphi_A = \pi - 2 \cos^{-1} \left(\frac{1.391}{\pi M d} \right)$ is the broadside HPBW of a ULA [44], and $\Theta_A = (\varphi_A/2) \sqrt{(10/3) \log_{10}[G_1(\phi)/G_2]}$ is the main lobe beamwidth of the approximated array radiation pattern corresponding to a specific value of ϕ . The peak mainlobe gain, G_1 , and the average side lobe gain, G_2 , are kept the same as the flat-top pattern. While the value of G_1 depends on the element pattern, the value of G_2 does not [36]. The value of G_2 is, therefore, the same with the directional element as with the isotropic element. Thus, for a ULA, these values are computed using [45] as

$$G_1(\phi) = G_e(\phi) M, \quad G_2 = \frac{1}{M \sin^2 \left(\frac{3\pi}{2M} \right)}. \quad (8)$$

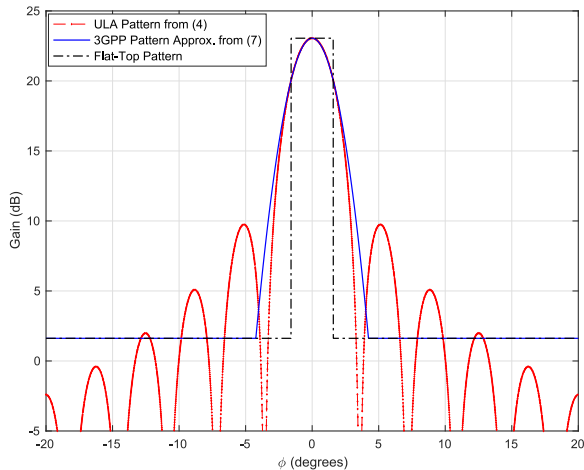


Fig. 2. Different antenna array radiation patterns for a ULA with 32 elements and steered to broadside, i.e., $\theta = 0^\circ$.

With the 3GPP array pattern approximation, we may finally express our effective scalar channel model as $\sqrt{L_k(r)}\tilde{G}_A(\phi, \theta)\varrho_k$.

Fig. 2 illustrates the relation between the proposed 3GPP array pattern approximation, the ULA pattern given in (4), and the flat-top pattern when the array is steered to broadside, i.e., $\theta = 0^\circ$. As compared to the flat-top pattern, the proposed 3GPP pattern approximation better models the main lobe. While the flat-top pattern accurately models the peak main lobe gain at a specific steering angle, it does not result in a reduction of the array gain because of small alignment errors around that steering direction. For alignment errors exceeding the HPBW, however, the array gain is reduced to the minimum value. These result in overestimation of the actual SNR in the case of small alignment errors and an underestimation of SNR when the alignment errors are significant, as will be shown in Section V.

G. Beam Alignment Error Model

We assume that the channel for downlink beamforming is estimated using the uplink pilot signals transmitted by the UE [46]. The tagged BS estimates the AoA from the uplink received SNR and steers the beam towards the desired direction. With perfect beam alignment, the downlink array gain equals the maximum boresight gain, $G_1(\phi)$, corresponding to a specific value of ϕ . However, perfect beam alignment is hard to realize due to inaccurate AoA estimation, which results in beam alignment errors. Since we are interested in the array gain corresponding to a specific direction, ϕ , we set the beam alignment error to be $\epsilon = (\phi - \theta)$ in (7) and express the array response as $\tilde{G}_A(\phi, \epsilon)$ in the remainder of this work.

The statistics of the beam alignment error, ϵ , are typically modeled using the truncated Gaussian distribution with zero mean [25]. Similar to [16], the PDF of such a distribution is expressed as

$$f_\epsilon(y) = \frac{\sqrt{\frac{2}{\pi\sigma_\epsilon^2}} \exp\left(-\frac{y^2}{2\sigma_\epsilon^2}\right)}{\operatorname{erf}\left(\frac{\pi/3}{\sqrt{2}\sigma_\epsilon}\right) - \operatorname{erf}\left(\frac{-\pi/3}{\sqrt{2}\sigma_\epsilon}\right)}, \quad y \in \left[-\frac{\pi}{3}, \frac{\pi}{3}\right] \quad (9)$$

where $\operatorname{erf}(\cdot)$ is the error function [47], σ_ϵ is the standard deviation of the beam alignment error and the domain of ϵ is equal to the angular space covered by one BS sector. Though, it was mentioned in [16] that a large value of σ_ϵ results in a greater alignment error, prior works assumed a constant value of σ_ϵ for all the UEs without specifying how σ_ϵ is obtained.

In this work, we use the CRLB of the AoA estimates to obtain σ_ϵ . The CRLB is a theoretical bound that gives the lowest estimation variance of any unbiased estimator and is obtained by inverting the corresponding Fisher Information (FI) [48]. The CRLB, however, is dependent on the underlying system model. Specifically, for AoA estimation, the CRLB depends on the number of antenna elements in the array, the spacing between the individual antenna elements, the array geometry, the array orientation with respect to the impinging wave, the underlying channel and the received SNR of the pilot signal [49]. For a very similar system model as ours, i.e., a single path channel (which represents the dominant propagation path) and a ULA with half-wavelength spaced antenna elements (where the direction of arrival of the incoming wave is measured from the boresight of the array), a closed-form expression for the CRLB of AoA estimates has been derived in [49] as a function of the SNR of the received pilot signal. Using the said expression of the CRLB corresponding to AoA estimation for a ULA, we express the variance of the beam alignment error for channel state k as

$$\sigma_{\epsilon_k}^2(\phi, \gamma_k) = \frac{6}{\left(\frac{2\pi f_c d \cos(\phi)}{c}\right)^2 M(M-1)\gamma_k}, \quad (10)$$

where f_c is the carrier frequency, c is the speed of light, ϕ is the true AoA and γ_k is the uplink received SNR at a single BS antenna element. In [49], γ_k was characterized for an omnidirectional element pattern and channel coefficients that follow a complex Gaussian distribution. However, since we adopt a Nakagami fading model and consider directional element patterns, our characterization of γ_k is more involved. In our model, the uplink SNR and the true AoA are dependent as the former is a function of the latter. If the typical UE is served by a BS with channel state k , then γ_k can be formulated as

$$\gamma_k(\phi, x) = \frac{P_u G_e(\phi) \varrho_k^{ul} L_k(x)}{\sigma_n^2}, \quad (11)$$

where P_u is the uplink transmit power, ϱ_k^{ul} is the channel gain due to small-scale fading experienced by the pilot signals and σ_n^2 is the noise power. For the simulations of the aforementioned CRLB-based beam alignment error model, we use (9) along with (10) and (11) to generate the alignment error. In Section III-B, we show that (9) – (11) give rise to a truncated Student's t -distribution, whose statistics are employed in our mathematical analysis.

The aforementioned CRLB-based approach for modeling the beam alignment errors renders the lowest possible values of such errors because of the definition of the CRLB. Hence, the downlink SNR performance derived in Section III (using the proposed CRLB model) serves as an upper bound for any practical beam alignment algorithm. To validate the SNR findings obtained using our proposed CRLB-based approach, we also simulate a practical beam alignment algorithm provided

TABLE I
NOTATION AND DEFAULT SYSTEM PARAMETERS

Notation	Description	Value
λ_B	BS density	50/km ²
λ_U	User density	200/km ²
P_d	Downlink transmit power	30 dBm
P_u	Uplink transmit power	23 dBm
f_c	Carrier frequency	28 GHz
W	Bandwidth	1 GHz
α_L, α_N	LOS and NLOS path loss exponents respectively	2, 2.92
C_L, C_N	LOS and NLOS path loss intercepts respectively	-61.4 dB, -72 dB
N_L, N_N	Nakagami shape parameters for LOS and NLOS signals	3, 2
σ_n^2	Noise power	-174 dBm/Hz + 10 log ₁₀ (W) + 10 dB
μ, R_B	LOS ball model parameters	0.2, 200 m

in [15], which considers a ULA at the BS and an omnidirectional antenna at the UE. We choose [15] for comparison because of its robustness and low implementation complexity, as claimed therein. For the purpose of fair comparison, we modify the code made available by the authors of [15] to suit our system model, i.e., we restrict to a single path channel with Nakagami fading, avoid beamforming with a single RF chain, and we include the effects of blockage and directional antennas elements.

By using a set of multiple sparse bipartite graphs (SBG), [15] formulates the beam alignment problem as a sparse encoding and phaseless decoding problem. Specifically, the sparse mm-wave channel is represented in the beam domain using a discrete Fourier Transform (DFT) matrix whose dimensions equal the number of antenna elements at the BS. Each column of the DFT matrix represents a beamforming vector for a particular direction. The BS probes the channel using these beamforming vectors and compressive phaseless measurements are collected along different directions. An estimate of the optimal beamforming direction for the desired user is then obtained from the magnitude information of these measurements, which depend on the channel SNR.

The system parameters used in this paper are summarized in Table I, where all the values, except λ_B , are adopted from [37]. The values of λ_B used in this work correspond to a noise-limited network [7], [9], in which the signal-to-interference-plus-noise ratio (SINR) is the same as the SNR. Therefore, we only deal with SNR in this paper.

III. DOWNLINK SNR COVERAGE PROBABILITY

This section gives the analytical formulation of the downlink SNR coverage probability, $\mathcal{C}(\tau)$, with imperfect beam alignment and is the main technical contribution of this paper. $\mathcal{C}(\tau)$ represents the probability that the *downlink* received SNR, Ω , at any location in the network is greater than a certain threshold τ , i.e., $\mathcal{C}(\tau) = \mathbb{P}(\Omega > \tau)$. For the typical user, the conditional downlink SNR coverage probability, $\mathcal{C}_k(\tau)$, conditioned on channel state k , is expressed as

$$\mathcal{C}_k(\tau) = \mathbb{P}(\Omega > \tau | k) \triangleq \mathbb{P}\left(\frac{P_d \tilde{G}_A(\phi, \epsilon) \varrho_k^{dl} L_k(x)}{\sigma_n^2} > \tau \mid k\right), \quad (12)$$

where ϱ_k^{dl} is the small-scale fading gain on the downlink with channel state k . It is worth mentioning here that with our system model, where the channel state information (CSI) for downlink beamforming is obtained from uplink pilots, the downlink fading gain is the same as the corresponding gain on the uplink due to channel reciprocity. However, since small-scale fading has a minimal impact on the performance of mm-wave systems [10], ϱ_k^{dl} is assumed to be independent of ϱ_k^{ul} in this section to enable mathematical analysis. Nevertheless, such an assumption does not create any disparity as will be validated with the help of simulations in Section V.

Because the downlink steering error depends on uplink SNR, a dependence exists between the downlink and uplink SNRs [42]. This is because the location and orientation of the tagged BS (from the typical UE's perspective) remain the same during the AoA estimation and downlink data transmission phases. Notice that ϕ and x both are present in (11) and (12). It is, therefore, important to incorporate such a dependence in the beam alignment error analysis. Our earlier analytical approach in [27], however, ignored such a dependence. To this effect, we develop a novel analytical approach in this section to obtain the downlink SNR coverage probability. To distinguish the two approaches from each other, we term the approach of [27] as 'averaging out ϕ approach' and the approach developed in this paper as the 'Student's t -distribution based approach'. The two approaches differ in the way the variance of the beam alignment error is used in the analysis. In the following, we first briefly discuss the former approach by highlighting its limitations and then motivate and justify the need for the latter.

A. Approach Based on Averaging Out ϕ [27]

This approach aims to facilitate the mathematical analysis by simplifying the expression for the variance, $\sigma_{\epsilon_k}^2$ of the beam alignment error and restricting the alignment errors to the main lobe of the array pattern, i.e., $|\epsilon| \leq \Theta_A$. Since the CRLB from (10) depends on two parameters, ϕ and γ_k , the dependence on ϕ is averaged out in this approach, thus, rendering $\sigma_{\epsilon_k}^2$ dependent on uplink SNR only. To accomplish this averaging, the joint PDF of ϕ and γ_k is first derived, which involves an integral over x . Using this joint PDF, ϕ is averaged out from $\sigma_{\epsilon_k}^2$. The overall simplification process for $\sigma_{\epsilon_k}^2$, thus, requires integration to be performed over both ϕ and x and eliminates the explicit dependence of the beam alignment error on both these RVs.

Lemma 1: With $|\epsilon| \leq \Theta_A$ and using the simplified expression for $\sigma_{\epsilon_k}^2$, which depends on uplink SNR only, the conditional downlink SNR coverage probability with imperfect beam alignment is obtained as

$$\mathcal{C}_k(\tau) \approx - \sum_{n=1}^{N_k} (-1)^n \binom{N_k}{n} \int_0^\infty \int_\phi \int_g e^{\left(\frac{-\beta_k n \tau \sigma_n^2}{P_d g L_k(x)}\right)} \times f_{\tilde{G}_A}(g|\phi) dg f_\phi(\phi) d\phi \hat{f}_k(x) dx, \quad (13)$$

where $\beta_k = N_k(N_k!)^{\frac{1}{N_k}}$, $f_\phi(\phi) = \frac{3}{2\pi}$ since ϕ is assumed to be distributed uniformly within its interval, $\hat{f}_k(x)$ represents the conditional PDF of the distance between the typical user and its serving BS conditioned on the BS belonging to the k^{th} channel

state and $f_{\tilde{G}_A|\phi}(g|\phi)$ is the conditional PDF of the array gain which is expressed as

$$f_{(\tilde{G}_A|\phi)}(g|\phi) = 2f_{\epsilon_k} \left(\sqrt{\frac{-5}{6} \log_{10} \left(\frac{g}{G_1(\phi)} \right)} \varphi_A \right) \times \frac{5}{12} \frac{\varphi_A}{\sqrt{\frac{-5}{6} \log_{10} \left(\frac{g}{G_1(\phi)} \right)}} \frac{1}{g \ln(10)} \quad (14)$$

for $g \in [G_2, G_1(\phi)]$.

Proof: The proof is given in [27] and omitted here for conciseness. ■

The value of $\hat{f}_k(x)$ is given in [37] as

$$\hat{f}_k(x) = \frac{f_k(x)}{\mathcal{A}_k} \exp \left(-2\pi\lambda_B \int_0^{\chi_k(x)} t (1 - \mathcal{P}_k(t)) dt \right), \quad (15)$$

where $\chi_L(x) = \left(\frac{C_N}{C_L} \right)^{\frac{1}{\alpha_N}} (x)^{\frac{\alpha_L}{\alpha_N}}$, $\chi_N(x) = \left(\frac{C_L}{C_N} \right)^{\frac{1}{\alpha_L}} (x)^{\frac{\alpha_N}{\alpha_L}}$, $f_k(x)$ is the PDF of the distance to the nearest BS belonging to channel state k and \mathcal{A}_k is the probability of association with such a BS and expressed respectively as [37]

$$f_k(x) = 2\pi\lambda_B x \mathcal{P}_k(x) \exp \left(-2\pi\lambda_B \int_0^x x \mathcal{P}_k(x) dx \right), \quad (16)$$

$$\mathcal{A}_k = \int_0^\infty f_k(x) \exp \left(-2\pi\lambda_B \int_0^{\chi_k(x)} t (1 - \mathcal{P}_k(t)) dt \right) dx. \quad (17)$$

It is important to mention here that since the downlink SNR also depends upon ϕ and x , the integration over the entire probability space of these two parameters has to be performed twice in this approach, first during the simplification of CRLB and then in (13). This increases the computational complexity. The increased complexity makes it difficult to extend the approach of (13) to other performance metrics such as the rate coverage probability. Moreover, this approach restricts the alignment error to the main lobe of the array pattern.

B. Student's t -Distribution Based Approach

To overcome the aforementioned limitations of the above approach, we develop a thorough analytical approach in this section which is computationally more efficient and allows beam alignment errors to take on values in the interval $[-\pi/3, \pi/3]$. The computational efficiency is required to make the rate coverage computations more practical. This approach exploits the statistical properties of the beam alignment errors and eliminates the need for the intermediate probability distribution of the array gain and the joint distribution of ϕ and γ_k . Hence, it better models the dependence between uplink and downlink SNRs as it preserves the dependence of the beam alignment error on ϕ and x . From (10) and (11), the variance of the beam alignment errors can be expressed as a function of three independent RVs

ϕ , x and ϱ_k^{ul} as

$$\sigma_{\epsilon_k}^2(\varrho_k^{ul}, \phi, x) = \frac{6\sigma_n^2 \left(\frac{c}{2\pi f_c d} \right)^2}{\cos^2(\phi) M(M-1) P_u G_e(\phi) \varrho_k^{ul} L_k(x)}. \quad (18)$$

The expression of $\sigma_{\epsilon_k}^2$ given in (18) implies that the truncated Gaussian distribution of (9) becomes a compound distribution since its variance itself is a RV. Conditioned on all the three RVs which define $\sigma_{\epsilon_k}^2$, the truncated Gaussian distribution is rewritten as

$$f_{\epsilon_k|\varrho_k^{ul}, \phi, x}(y|z, \phi, x) = \frac{\sqrt{\frac{2}{\pi\sigma_{\epsilon_k}^2(z, \phi, x)}} \exp\left(\frac{-y^2}{2\sigma_{\epsilon_k}^2(z, \phi, x)}\right)}{\text{erf}[\zeta(z, \phi, x)] - \text{erf}[-\zeta(z, \phi, x)]}, \quad (19)$$

where $y \in [-\pi/3, \pi/3]$, i.e., the angular region of support for the beam alignment errors spans the entire BS sector and $\zeta(z, \phi, x) = \pi/(3\sqrt{2}\sigma_{\epsilon_k}^2(z, \phi, x))$. For succinctness, we do not express the region of support in the rest of the mathematical analysis, unless necessary. The expression in (19) is quite complicated to deal with due to the presence of the three RVs in both the numerator and the denominator. Further, the dependence on these RVs has to be preserved and cannot be integrated out at this stage. Marginalizing ϕ at this stage would eliminate the dependence of ϵ on it but not the dependence of $\tilde{G}_A(\phi, \theta)$. Same reasoning holds for the RV x ; the location of the tagged BS remains the same during the uplink pilot transmission and the downlink data transmission.

While the conditioning on ϕ and x cannot be eliminated in (19) because of the dependence between the uplink and downlink SNRs, ϱ_k^{ul} can be marginalized since small-scale fading has a minimal impact on mm-wave systems [10]. Thus, the conditional distribution of the beam alignment error given only ϕ and x can be written as

$$f_{\epsilon_k|\phi, x}(y|\phi, x) = \int_0^\infty f_{\epsilon_k|\varrho_k^{ul}, \phi, x}(y|z, \phi, x) f_{\varrho_k^{ul}}(z; N_k, N_k) dz, \quad (20)$$

where $f_{\varrho_k^{ul}}(z; N_k, N_k)$ is given in (3). The above integral is quite exhaustive to calculate numerically. However, the form of (20), specifically a truncated Gaussian distribution compounded with a gamma distribution, becomes a truncated Student's t -distribution [50]. The Student's t -distribution (henceforth referred to as only ' t -distribution') is a continuous probability distribution whose shape resembles that of a Gaussian distribution but has relatively fatter tails. Equation (20) can thus be expressed in the form of a scaled t -distribution as

$$f_{\epsilon_k|\phi, x}(y|\phi, x) := \frac{\frac{1}{\delta(\phi, x)} f_t\left(\frac{y}{\delta(\phi, x)}\right)}{F_t\left(\frac{\pi/3}{\delta(\phi, x)}\right) - F_t\left(-\frac{\pi/3}{\delta(\phi, x)}\right)}, \quad (21)$$

where $y \in [-\pi/3, \pi/3]$, and $f_t(\cdot)$ and $F_t(\cdot)$ are the PDF and cumulative distribution function (CDF) of a standardized

t -distribution, respectively and given in [51] as

$$f_t(y) = \frac{\Gamma\left(\frac{\nu+1}{2}\right)}{\Gamma\left(\frac{\nu}{2}\right)} \frac{1}{\sqrt{\nu\pi}} \frac{1}{\left(1 + \frac{y^2}{\nu}\right)^{\frac{\nu+1}{2}}}, \quad (22)$$

$$F_t(y) = \frac{1}{2} + y \Gamma\left(\frac{\nu+1}{2}\right) \frac{{}_2F_1\left(\frac{1}{2}, \frac{\nu+1}{2}; \frac{3}{2}; -\frac{y^2}{\nu}\right)}{\sqrt{\nu\pi} \Gamma\left(\frac{\nu}{2}\right)}, \quad (23)$$

where ν is called the *degrees of freedom* of the t -distribution and ${}_2F_1(\cdot)$ is the Gauss hypergeometric function. The parameter ν equals twice the shape parameter of the underlying gamma distribution, i.e., $\nu = 2N_k$. The factor $\delta(\phi, x)$ is a scale parameter of the t distribution and is a function of two RVs ϕ and x . From (18), $\delta(\phi, x)$ can be written as

$$\delta(\phi, x) = \sqrt{\frac{6\sigma_n^2}{\left(\frac{2\pi f_c d \cos(\phi)}{c}\right)^2 M(M^2 - 1) P_u G_e(\phi) L_k(x)}}. \quad (24)$$

The expression in (21) can now be utilized in conjunction with (12) to derive the downlink SNR coverage probability. Following the approach of [8] and [16], $C_k(\tau)$ is reformulated from (12) as

$$\begin{aligned} C_k(\tau) &= \mathbb{P}\left(\varrho_k^{dl} > \frac{\tau\sigma_n^2}{P_d \tilde{G}_A(\phi, \epsilon) L_k(x)} \mid k\right) \\ &\stackrel{(a)}{\approx} 1 - \mathbb{E}_{x, \tilde{G}_A} \left(\left[1 - e^{-\frac{-\beta_k \tau \sigma_n^2}{P_d \tilde{G}_A(\phi, \epsilon) L_k(x)}} \right]^{N_k} \mid k \right) \\ &\stackrel{(b)}{\approx} - \sum_{n=1}^{N_k} (-1)^n \binom{N_k}{n} \mathbb{E}_{x, \tilde{G}_A} \left[e^{-\frac{-\beta_k n \tau \sigma_n^2}{P_d \tilde{G}_A(\phi, \epsilon) L_k(x)}} \right], \end{aligned} \quad (25)$$

where $\beta_k = N_k(N_k!)^{-\frac{1}{N_k}}$, (a) is obtained by using the CDF approximation of the gamma RV and (b) follows by applying the Binomial theorem [8]. The downlink array gain is a function of two RVs, ϕ and ϵ ; therefore, the expectation over it can be evaluated using the distributions of ϕ and ϵ . Thus, (25) can be expressed as

$$\begin{aligned} C_k(\tau) &:= - \sum_{n=1}^{N_k} (-1)^n \binom{N_k}{n} \\ &\times \int_{x=0}^{\infty} \int_{\phi=-\frac{\pi}{3}}^{\frac{\pi}{3}} \int_{\epsilon=-\frac{\pi}{3}}^{\frac{\pi}{3}} e^{-\frac{-\beta_k n \tau \sigma_n^2}{P_d \tilde{G}_A(\phi, \epsilon) L_k(x)}} \\ &\times f_{\epsilon|\phi, x}(y|\phi, x) f_{\phi}(\phi) \hat{f}_k(x) d\epsilon d\phi dx, \end{aligned} \quad (26)$$

where $\tilde{G}_A(\phi, \epsilon)$ depends on the number of antenna elements as per (7) – (8), $f_{\epsilon|\phi, x}(y|\phi, x)$ is given above in (21) and $\hat{f}_k(x)$ is given in (15). From the law of total probability, the total downlink SNR coverage is expressed as $\mathcal{C}(\tau) = \sum_k \mathcal{A}_k C_k(\tau)$.

In the t -distribution based approach, the scale parameter, $\delta(\phi, x)$, captures the location and orientation of the tagged BS during the AoA estimation phase. The integration over ϕ and x

is performed only at the very last step, thus, accurately modeling the correlation between uplink and downlink SNRs.

The effect of ϕ models the scan loss due to the antenna element pattern. While the integrals over ϵ and x can be computed easily numerically using the `integral` function in MATLAB[®], the integration over ϕ is computationally intense. This is because the uplink SNR, the peak main lobe gain of the array pattern in downlink and the corresponding main lobe beamwidth, all depend on ϕ . The integral over ϕ is, therefore, approximated using the Gauss-Legendre quadrature. The Gauss-Legendre quadrature approximates the value of a definite integral by converting it into a weighted sum of orthogonal polynomials. Specifically, the numeric value of a definite integral of a function can be approximated by Gauss-Legendre quadrature as follows

$$\int_a^b f(y) dy \approx \frac{b-a}{2} \sum_{q=1}^Q w_q f(y_q), \quad (27)$$

where $y_q = \left(\frac{b-a}{2}\right)z_q + \frac{b+a}{2}$, z_q is the q^{th} zero of the N^{th} order Legendre polynomial and w_q is the corresponding value of the weight. The values of z_q and w_q have been tabulated in [47] for various values of Q . For this research, a value of $Q = 12$ gives a reasonable accuracy with acceptable computational complexity.

IV. DOWNLINK RATE COVERAGE PROBABILITY

In this section, the downlink achievable rate in a mm-wave cellular network is characterized in the presence of beam alignment errors. The per user rate depends on the SNR of the link. Another factor that plays a critical role is the fraction of the time-frequency resources available to a user, which depends on the load on the serving BS. The load represents the number of users sharing the total available resources of a BS. In the following, we first explain how the load is analytically characterized for our system model, and then describe the calculation of the achievable rate. Afterwards, we define the metric of *rate coverage probability* and show how it can be analytically obtained from the results of SNR coverage probability derived in Section III-B.

In a Poisson distributed network, the load is a RV which depends on the user-to-BS association strategy [52]. The association strategy defines the association regions of respective BSs. The notion of the association region of a BS is the same as the cell formed by that BS. To analytically characterize the load, the size/area of a BS's association region is required, which itself is a RV. Because of these reasons, formulating the exact load distribution in a Poisson distributed network is an open problem [10]. For sub-6 GHz networks, the load distribution is approximated using the statistics of Poisson-Voronoi tessellations. In mm-wave networks, however, there are more intricacies as the blockage effects lead to association regions that are disjoint and irregularly shaped [2]. Moreover, the use of the ball blockage model renders the original BS PPP as two non-homogeneous PPPs [37], which are difficult to deal with analytically. Thus, it has been argued extensively in the existing literature that the load distribution of the sub-6 GHz networks can also be used for mm-wave networks to analyze

the achievable rate. The approximate probability mass function (pmf) of the load, N , on the tagged BS of a mm-wave network is expressed as [2]

$$\mathbb{P}[N = n] = \frac{3.5^{3.5}}{(n-1)!} \frac{\Gamma(n+3.5)}{\Gamma(3.5)} \left(\frac{\lambda_u}{\lambda_B}\right)^{n-1} \times \left(3.5 + \frac{\lambda_u}{\lambda_B}\right)^{-(n+3.5)}. \quad (28)$$

In this paper, we assume that the UEs associated to a BS are scheduled in a round-robin fashion and the total resources of the BS are divided equally among the connected UEs. Using Shannon's capacity formula, the per user rate conditioned on channel state k is then expressed as

$$R_k = \frac{W}{N} \log_2(1 + \Omega_k) \quad (29)$$

where W is the total bandwidth available at a BS and Ω_k is the SNR of the link. In general, Ω_k and N are not independent, however, modeling their correlation is highly complex [53]. For tractability of analysis, these two RVs are assumed to be independent [10]. To analyze the achievable rate in the network, a widely used metric is the rate coverage probability $\mathcal{R}_k(\rho)$. It is equal to the complementary CDF (CCDF) of R_k and represents the fraction of users that are able to meet predefined rate thresholds. Mathematically,

$$\begin{aligned} \mathcal{R}_k(\rho) &= \mathbb{P}[R_k > \rho] \stackrel{(a)}{=} \mathbb{P}\left(\Omega_k > 2^{\frac{\rho N}{W}} - 1\right) \\ &\stackrel{(b)}{=} \mathbb{E}_N \left[\mathcal{C}_k \left(2^{\frac{\rho N}{W}} - 1 \right) \right] \\ &\stackrel{(c)}{=} \sum_{n \geq 1} \frac{3.5^{3.5}}{(n-1)!} \frac{\Gamma(n+3.5)}{\Gamma(3.5)} \left(\frac{\lambda_u}{\lambda_B}\right)^{n-1} \\ &\quad \times \left(3.5 + \frac{\lambda_u}{\lambda_B}\right)^{-(n+3.5)} \mathcal{C}_k \left(2^{\frac{\rho N}{W}} - 1 \right) \end{aligned} \quad (30)$$

where $\mathcal{C}_k(\cdot)$ represents the SNR coverage obtained in Section III-B, (a) follows from (29), (b) is because the load is a RV and (c) is obtained by using the pmf of the load given in (28). The total rate coverage probability of the network is expressed as $\mathcal{R}(\rho) = \sum_k \mathcal{A}_k \mathcal{R}_k(\rho)$.

The expression in (30) shows that the rate coverage probability can be obtained analytically from the SNR coverage probability. Moreover, the summation involves infinite terms but as shown in [9], fairly accurate results can be obtained by considering a finite maximum number of terms depending on the ratio of user to BS densities. For the densities of Table I, it has been observed that considering the first 24 terms is sufficient. Since calculation of \mathcal{R}_k for a single value of ρ requires multiple computations of the SNR coverage probability, we use the t -distribution based approach as it is computationally more efficient.

V. RESULTS AND DISCUSSION

In this section, the performance of a mm-wave cellular network is evaluated in the presence of beam alignment errors, which are modeled according to our proposed CRLB-based approach, and the analytical results are verified using simulations.

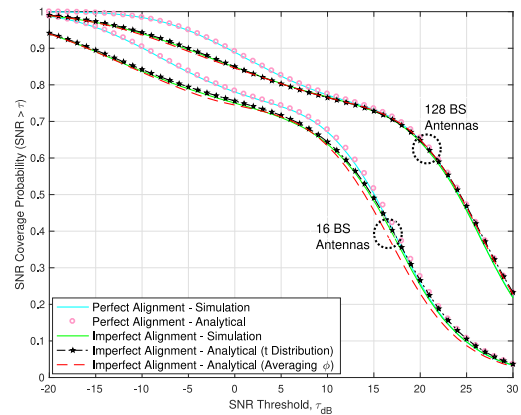


Fig. 3. Comparison of the two analytical approaches for downlink SNR coverage probability with different numbers of antenna elements (M) at a BS density (λ_B) = 50/km². Alignment errors restricted to main lobe beamwidth.

For the simulations, 10⁵ Monte-Carlo trials are conducted and the small-scale fading gain on the downlink is considered to be the same as the corresponding gain on the uplink.

In the following, we start by discussing the results of downlink SNR coverage probability in the presence of beam alignment errors. Initially, we show how the perfect alignment coverage compares with imperfect alignment coverage when the beam alignment errors are confined to the mainlobe beamwidth. Then, we illustrate the effect of expanding the region of support of such errors. After that, we compare the effects of increasing the number of BS antennas and the BS density where such a comparison is also done for the case of SBG beam alignment algorithm. We then illustrate how the rate coverage probability is affected in the presence of beam alignment errors. The effects of increasing the number of BS antennas and the BS density are compared for the rate coverage as well. At the end, we show how our proposed 3GPP array pattern approximation compares with the flat-top array pattern in terms of SNR coverage and rate coverage with imperfect beam alignment. For the purpose of clarity, it is worth mentioning that the CRLB method for beam alignment errors is used in all of the following figures, whereas the SBG algorithm is used only in Fig. 5.

Fig. 3 shows the downlink SNR coverage probability with perfect and imperfect beam alignment for two different array sizes and aims to compare the performance of the two analytical approaches mentioned in Section III. As a reminder, the analytical approach based on ‘averaging out ϕ ’ does not render itself to model the beam alignment errors in the interval $[-\pi/3, \pi/3]$. Therefore, for a fair comparison, the beam alignment errors are restricted to the main lobe beamwidth, i.e., Θ_A of the array pattern for all the curves. To reflect such a restriction, a parameter of the t -distribution based approach in (19) is slightly modified as $\zeta(z, \phi, x) = \Theta_A / (\sqrt{2}\sigma_{\epsilon_k}^2(z, \phi, x))$. The analytical curves for perfect alignment are obtained from (26) simply by replacing $\tilde{G}_A(\phi, \epsilon)$ with $\tilde{G}_A(\phi)$ and ignoring the integral over ϵ along with $f_{\epsilon|\phi, x}$. It is observed in Fig. 3 that the analytical curves obtained from both the approaches match very well with the corresponding simulated curves. This verifies that the assumption of independent small-scale fading gain on the uplink and the downlink is reasonable and does not create any

disparity in the analysis. The closeness of the analytical curves also illustrates that averaging out ϕ from $\sigma_{\epsilon_k}^2$ (as done in [27]) has a relatively minor impact on the beam alignment error. In comparison with the approach of [27], however, the curve obtained from the t -distribution based approach is closer to the simulated curve for most values of τ and follows the trend of the simulated curve better for both the array sizes. This substantiates our claim that the t -distribution based analytical approach is more precise since it accurately models the dependence between the uplink and downlink SNRs. Therefore, in the rest of this section, the t -distribution based approach is employed to obtain the analytical curves.

For a specific BS density, there exists a particular value of the coverage probability beyond which the achievable SNR decays rapidly. This trend is because of the ball blockage model. For example, in Fig. 3 with $\lambda_B = 50/\text{km}^2$, $M = 16$, and perfect alignment, a coverage probability of 0.74 reflects such a value. The corresponding value of τ is 5 dB, which represents the average SNR at the boundary of LOS ball with such an array configuration. Smaller values of τ are representative of the NLOS UEs, which are outside the LOS ball, whereas larger values of τ represent the UEs which are inside the ball and have a certain probability of LOS connectivity.

For perfect alignment, the SNR coverage with $M = 128$ is simply a right shifted version of the coverage with $M = 16$. The amount of shift is equal to the difference between the array gains for the two configurations, i.e., 9 dB in Fig. 3.

The same, however, is not true for the coverage probabilities with imperfect alignment. For $\tau < 5$ dB, where systems using error correction codes are likely to operate, the difference between the perfect alignment coverage and imperfect alignment coverage is quite high for both antenna configurations. This difference tends to decrease as the system transitions towards a high SNR regime and almost vanishes at a certain value of τ . However, for $M = 128$, the difference vanishes at a comparatively smaller value of τ . For example, at coverage probability equal to 0.8, the difference between the perfect and imperfect alignment curves is about 5 dB for $M = 16$. The same difference comes out to be 2 dB for $M = 128$. This is because the variance of beam alignment errors is inversely proportional to M^3 as shown in (10).

While increasing M reduces the effects of beam alignment errors, the reduction is more pronounced for high SNR regime as compared to the low SNR regime. Increasing M from 16 to 128 reduces the difference between perfect alignment coverage and imperfect alignment coverage by about 3 dB at a coverage probability of 0.7 but only by 1 dB at a coverage probability of 0.9. The above discussion implies that the beam alignment errors degrade the performance of a mm-wave network significantly in low SNR regime (i.e., for NLOS UEs) as compared to high SNR regime (i.e., for LOS UEs); and increasing the number of antennas does not completely eliminate this degradation of performance.

The different performance effects for the LOS and NLOS UEs can be explained based on the beam alignment error variance, $\sigma_{\epsilon_k}^2$. As shown in (10), $\sigma_{\epsilon_k}^2$ is inversely proportional to the received SNR, γ_k , of the uplink pilot signals. For NLOS UEs, γ_k is low because of the inherent channel conditions. This causes

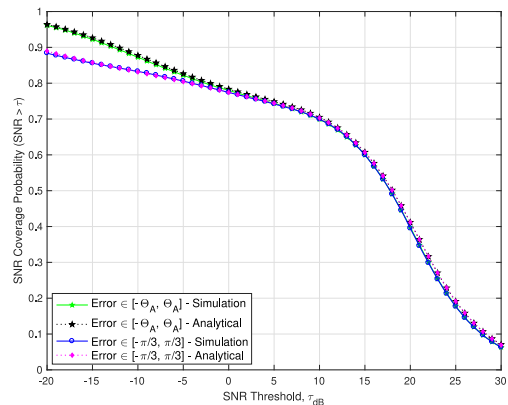


Fig. 4. Downlink SNR coverage probabilities with imperfect beam alignment for different regions of support of the beam alignment errors. Number of BS antennas (M) = 32, BS density (λ_B) = 50/km².

a larger value of $\sigma_{\epsilon_k}^2$, which in turn results in a large value for ϵ_k , as explained in Section II-G. A high value of ϵ_k reduces the array gain, $\tilde{G}_A(\phi, \epsilon)$, significantly in the desired direction. A reduction in the array gain consequently causes the downlink coverage probability to reduce, as derived in (26). For the LOS UEs, however, the relatively better channel conditions result in comparatively higher γ_k and a correspondingly lower value of ϵ_k ; in this case, the reduction in $\tilde{G}_A(\phi, \epsilon)$ because of the alignment errors is, therefore, minuscule and the coverage probability does not degrade much.

Fig. 4 illustrates how expanding the region of support for the beam alignment errors affects the downlink SNR coverage probability. When the beam alignment errors are not confined to the main lobe beamwidth, the distant/NLOS users are affected adversely whereas the users closer to the BS (or LOS users) do not experience any consequences. This is because the magnitude of the alignment errors for distant users is so huge that the associated BS fails to direct the main lobe at them and they are served instead by the sidelobes of the BS array. The observations from Fig. 4 illustrate that it is more realistic not to confine the alignment errors to the main lobe beamwidth. The observations also justify the need for developing the t -distribution based analytical approach which can effectively model the beam alignment errors in any interval. In the following discussion, the beam alignment errors span the interval $[-\pi/3, \pi/3]$.

Fig. 5 compares the effects of increasing the BS density and increasing the number of BS antennas on the SNR coverage with imperfect alignment. Along with the simulation and analytical curves obtained with our proposed CRLB-based approach, also shown here are the curves obtained with the SBG algorithm of [15]. The solid curves represent the simulations of the CRLB approach and the dotted curves with markers represent our proposed analytical approach that also uses the CRLB. The SBG curves are represented with dashed dotted lines. Two sets of curves (red and black colored) have the same $\lambda_B = 50/\text{km}^2$ and differ only in the value of M while one set of curves (green colored) has $M = 32$ and $\lambda_B = 70/\text{km}^2$. In the following, we first discuss the simulation and analytical results obtained with the CRLB-based approach, and then we explain the curves obtained by simulating the SBG algorithm.

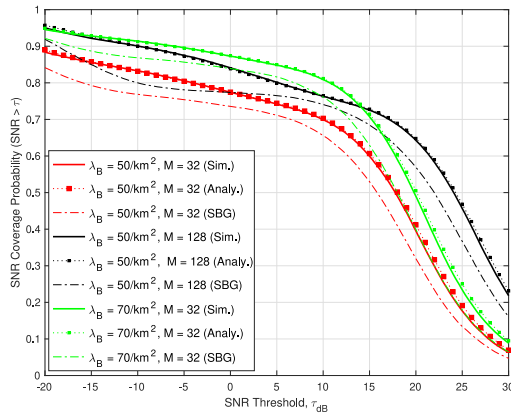


Fig. 5. Downlink SNR coverage probability with imperfect alignment for varying number of BS antennas (M) and BS densities (λ_B). Beam alignment error (ϵ) $\in [-\frac{\pi}{3}, \frac{\pi}{3}]$.

For the CRLB-based method, we see that the analytical results match well with the simulations for all cases. With $M = 32$, for both $\lambda_B = 50/\text{km}^2$ and $\lambda_B = 70/\text{km}^2$, the average SNR at the boundary of the LOS ball is 10 dB. However, the coverage with $\lambda_B = 50/\text{km}^2$ is only about 70% at $\tau = 10$ dB and $M = 32$, while it is more than 81% with $\lambda_B = 70/\text{km}^2$. This illustrates that by increasing λ_B from $50/\text{km}^2$ to $70/\text{km}^2$ (a 1.4 times increase), an additional 11% of users are brought strictly inside but near the boundary of the LOS ball, who were otherwise outside the ball. If λ_B is kept fixed at $50/\text{km}^2$ and instead M is increased from 32 to 128 (a 4 times increase), the SNR coverage only increases by 5.8% at $\tau = 10$ dB. This is because increasing M shifts the curve towards right and though it increases the average SNR inside and at the boundary of the LOS ball, it does not increase the fraction of users inside the LOS ball. For users already inside the LOS ball (which corresponds to large values of τ), however, increasing M is more beneficial as compared to increasing λ_B for the BS densities under consideration. Notice that the green and black sets of curves for the CRLB method intersect at around $\tau = 14$ dB. To overshadow the benefits of increasing M at large values of τ , λ_B has to be increased by an enormous amount. These observations illustrate that increasing the BS density and the number of antennas provide varying degrees of benefits. For $-10 \text{ dB} \leq \tau \leq 14 \text{ dB}$, increasing the BS density with a lower number of antennas per BS is more effective than increasing the number of antennas per BS with a lower BS density.

We now discuss the downlink SNR coverage probability obtained by simulating the SBG beam alignment algorithm (i.e., dashed dotted curves in Fig. 5). For a specific value of λ_B and M , we observe that the SNR coverage probability with the SBG algorithm is lower than the corresponding SNR coverage obtained with the CRLB-based method. This is as expected because of the explanation provided in Section II-G, i.e., characterizing the alignment error variance using the CRLB results in lowest possible values for the alignment errors and a higher downlink SNR coverage. However, when λ_B and M are increased, similar trends are exhibited by the SBG curves as the corresponding CRLB-based curves, though with slight scaling differences. Notice that

the green and black dashed-dotted curves intersect at a specific value of τ , which is close to $\tau = 14$ dB, where the corresponding CRLB-based curves intersect. These observations indicate that the insights obtained in a practical beam alignment scenario are similar to those obtained using our proposed CRLB-based model. Moreover, we also observe that increasing M results in an increased gap between the SBG curve and the corresponding CRLB-based curve for low values of τ . Consider the black colored curves for $-10 \text{ dB} \leq \tau \leq 0 \text{ dB}$. This is because the SBG algorithm suffers from some performance degradation with the increase of M , as mentioned in [15], and such a degradation is exacerbated in the low SNR regime. As M increases, the mainlobe beamwidth of the array pattern reduces along with the accuracy of the SBG scheme. Hence, the magnitude of the alignment error with the SBG scheme is such that the UE is served by the BS sidelobe rather than the mainlobe, thereby decreasing the SNR coverage. With the CRLB-based method, however, the magnitude of the alignment error in this SNR regime is comparatively small, corresponding to keeping the UE within the mainlobe.

The overhead associated with the SBG algorithm is quantified in terms of the number of phaseless measurements required for beam alignment. Based on the graph coding framework developed in [15] for the SBG algorithm, the number of measurements required for a single RF chain equals twice the number of antenna elements at the BS. The computational complexity of this algorithm also increases with the increase of antenna elements at the BS.

The above discussion establishes that modeling the beam alignment errors using the proposed CRLB method is an efficient way of evaluating the system-level performance of a mm-wave cellular network. Therefore, in the following, we only consider the CRLB method for beam alignment errors.

Below, we evaluate the effects of the beam alignment errors on the rate coverage probability. Fig. 6 compares the rate coverage probability with perfect and imperfect beam alignment for 32 BS antennas. The rate coverage with perfect alignment is greater as compared to the case with imperfect alignment, however, the difference between the two vanishes for higher rate threshold, ρ . This trend in the rate coverage is the same as with the SNR coverage (see Fig. 3). The higher rate thresholds are representative of LOS users whereas lower rate thresholds are typical of NLOS users. The results indicate that the beam alignment errors reduce the achievable rate of the NLOS users considerably whereas the effect on LOS users is negligible. The reason for this effect is the same as mentioned in the explanation of Fig. 3, i.e., NLOS users have a relatively higher beam alignment error variance and a correspondingly lower array gain in the desired direction, whereas LOS users have a comparatively lower beam alignment error variance and a relatively higher array gain in the desired direction. The achievable SNR for NLOS users is, therefore, lower as compared to LOS users. The same also holds for the achievable rate since rate is a monotonic function of the SNR, as per (29). As an example, we study the rate coverage at $\rho = 10^7$, which is typical to NLOS users outside the LOS ball. The rate coverage with perfect alignment at this value of ρ is almost 96% whereas the same with imperfect alignment is only 85%.

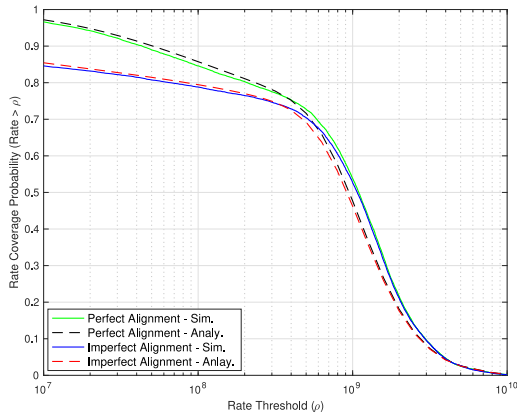


Fig. 6. Rate coverage probability for perfect and imperfect beam alignment with number of BS antennas (M) = 32 and BS density (λ_B) = 50/km². Beam alignment error (ϵ) $\in [-\frac{\pi}{3}, \frac{\pi}{3}]$.

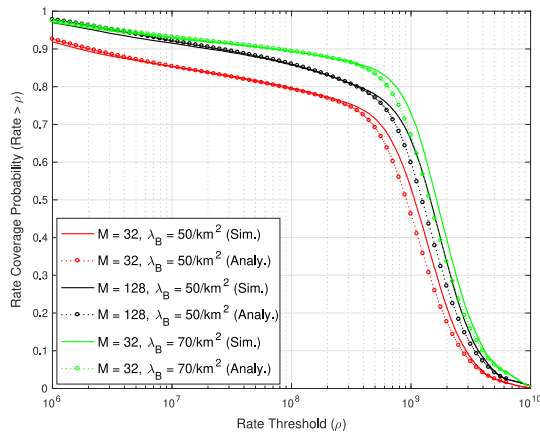


Fig. 7. Downlink rate coverage probability with imperfect alignment for varying number of BS antennas (M) and BS density (λ_B). Beam alignment error (ϵ) $\in [-\frac{\pi}{3}, \frac{\pi}{3}]$.

We also observe that the analytical curves match well with the simulations, however, a small gap starts to appear between them at almost $\rho = 5 \times 10^8$. This value of ρ represents the average achievable rate at the boundary of the LOS ball. The gap arises because of the approximate load distribution utilized in (30) and has also been observed in prior works on mm-wave networks, e.g., [9]. Despite the slight difference between the analytical and simulated curves, both the curves follow the same trends.

Fig. 7 compares the effects of increasing λ_B and M on the rate coverage probability with imperfect alignment. It is observed that increasing λ_B is more beneficial as compared to increasing M in order to reduce the effects of beam alignment errors. The findings here are different than the ones obtained from analyzing the SNR coverage only. Notice that the green and black curves here do not cross-over for higher thresholds, unlike Fig. 5. This is because increasing the BS density reduces the load on each BS in the network, which effectively increases the availability of the resources to each user. From (29), the effect of increasing the SNR on the rate is logarithmic whereas that of increasing the resource availability is linear. Therefore, while increasing the number of BS antennas to counter the alignment errors does

improve the SNR, it cannot outperform the benefits of increasing the BS density.

Fig. 8 compares the results obtained with the proposed 3GPP array pattern approximation and the flat-top pattern for $M = 32$ and $\lambda_B = 50/\text{km}^2$. With perfect beam alignment, the downlink SNR and rate provided by the flat-top pattern and the 3GPP approximation are identical as the peak main lobe gains of both are the same and the main lobe is pointed exactly in the desired direction. However, with beam alignment errors, the flat-top pattern overestimates the SNR coverage for large values of the SNR threshold, τ , and underestimates it for small values of τ . This is because the users close to the BS experience relatively small beam alignment errors and, hence, higher downlink SNR. Due to a flat main lobe in the flat-top pattern, small alignment errors do not result in any reduction of the array gain. On the other hand, the distant users experience comparatively large beam alignment errors and consequently poor downlink SNR because the array gain reduces to the sidelobe level. The observations from Fig. 8(a) verify that the flat-top pattern offers excessive gain penalty for large beam alignment errors.

The above-mentioned differences in the SNR coverage probability also cause differences in the rate coverage probability. As shown in Fig. 8(b), the rate coverage probability with flat-top pattern is lower than that obtained with the 3GPP pattern approximation for smaller values of the rate threshold, ρ . Distant users are only able to achieve low data rates due to poor SNR and larger beam alignment errors. The use of the flat-top antenna pattern for the analysis further penalizes such users. As an example, we study the achievable data rate at 81% rate coverage probability. With perfect beam alignment, 81% of the users are able to achieve at least 200.5 Mbps on average. However, with beam alignment errors and using the 3GPP pattern approximation, 81% of the users achieve at least 62.5 Mbps on average. If the flat-top pattern is used instead, then 81% of the users achieve at least 22.5 Mbps on average. A difference of 40 Mbps might not be significant for users that are close to their serving BSs and experience data rates in the Gbps range. However, for distant users operating near the edge of the cell (as in this case), a difference of 40 Mbps is huge. This observation necessitates the use of an accurate array approximation method for beam alignment error analysis.

VI. CONCLUSION

This paper studies the effects of beam misalignment on the downlink SNR and rate coverage probabilities of a mm-wave cellular network with particular attention to modeling. The beam alignment errors are modeled as a function of the SNR of the pilot signals transmitted during the channel estimation phase. An analytical approach in a tractable form and which preserves the dependence between the uplink and downlink SNRs is developed to obtain the downlink SNR coverage probability with imperfect alignment, which is then extended to the rate coverage probability. Our analysis and results illustrate that such alignment errors deteriorate the SNR and rate significantly for NLOS users whereas their effect is negligible for LOS users. With beam misalignment, increasing the number of antennas

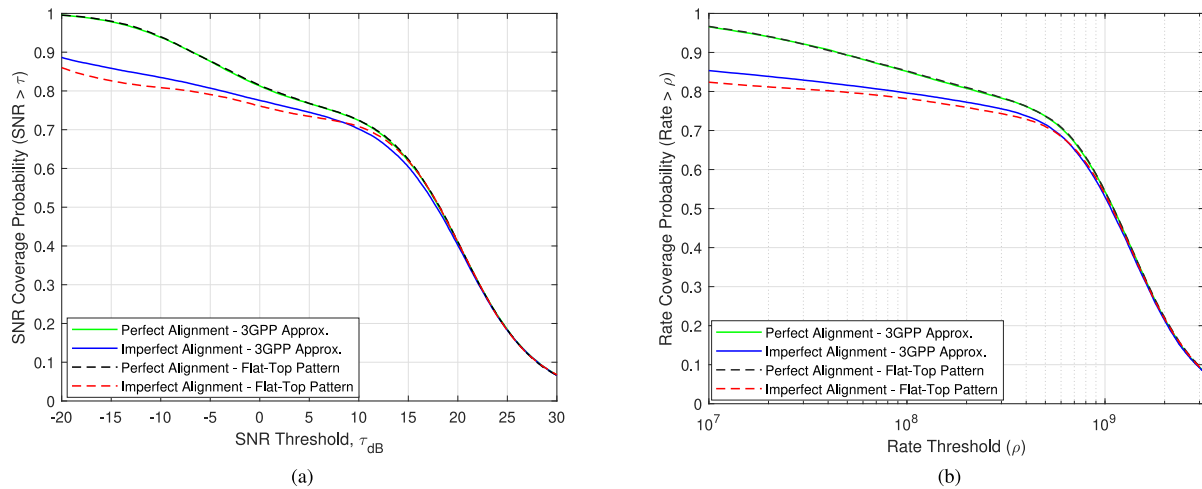


Fig. 8. Beam alignment error analysis with 3GPP pattern approximation vs. flat-top pattern (a) SNR Coverage Probability, (b) Rate Coverage Probability. BS density (λ_B) = $50/\text{km}^2$, number of BS antennas (M) = 32. Results obtained from simulations with beam alignment error (ϵ) $\in [-\frac{\pi}{3}, \frac{\pi}{3}]$.

increases the SNR coverage but does not alleviate the effects of alignment errors altogether. Moreover, increasing the BS density and the number of BS antennas benefit the SNR coverage in different ways. For rate coverage, however, it was observed that increasing the BS density is more beneficial than increasing the number of BS antennas. A comparison of the commonly used flat-top array pattern with our proposed 3GPP pattern approximation reveals that the former miscalculates the SNR and rate coverage in the presence of beam alignment errors.

REFERENCES

- [1] T. S. Rappaport, G. R. MacCartney, M. K. Samimi, and S. Sun, "Wideband millimeter-wave propagation measurements and channel models for future wireless communication system design," *IEEE Trans. Commun.*, vol. 63, no. 9, pp. 3029–3056, Sep. 2015.
- [2] S. Singh, M. N. Kulkarni, A. Ghosh, and J. G. Andrews, "Tractable model for rate in self-backhauled millimeter wave cellular networks," *IEEE J. Sel. Areas Commun.*, vol. 33, no. 10, pp. 2196–2211, Oct. 2015.
- [3] A. Ghosh *et al.*, "Millimeter-wave enhanced local area systems: A high-data-rate approach for future wireless networks," *IEEE J. Sel. Areas Commun.*, vol. 32, no. 6, pp. 1152–1163, Jun. 2014.
- [4] A. Alkhateeb, O. El Ayach, G. Leus, and R. W. Heath, "Channel estimation and hybrid precoding for millimeter wave cellular systems," *IEEE J. Sel. Topics Signal Process.*, vol. 8, no. 5, pp. 831–846, Oct. 2014.
- [5] M. R. Akdeniz *et al.*, "Millimeter wave channel modeling and cellular capacity evaluation," *IEEE J. Sel. Areas Commun.*, vol. 32, no. 6, pp. 1164–1179, Jun. 2014.
- [6] X. Yu, J. Zhang, M. Haenggi, and K. B. Letaief, "Coverage analysis for millimeter wave networks: The impact of directional antenna arrays," *IEEE J. Sel. Areas Commun.*, vol. 35, no. 7, pp. 1498–1512, Jul. 2017.
- [7] H. Elshaer, M. N. Kulkarni, F. Boccardi, J. G. Andrews, and M. Dohler, "Downlink and uplink cell association with traditional macrocells and millimeter wave small cells," *IEEE Trans. Wireless Commun.*, vol. 15, no. 9, pp. 6244–6258, Sep. 2016.
- [8] T. Bai and R. W. Heath, "Coverage and rate analysis for millimeter-wave cellular networks," *IEEE Trans. Wireless Commun.*, vol. 14, no. 2, pp. 1100–1114, Feb. 2015.
- [9] M. N. Kulkarni, A. Ghosh, and J. G. Andrews, "A comparison of MIMO techniques in downlink millimeter wave cellular networks with hybrid beamforming," *IEEE Trans. Commun.*, vol. 64, no. 5, pp. 1952–1967, May 2016.
- [10] J. G. Andrews, T. Bai, M. N. Kulkarni, A. Alkhateeb, A. K. Gupta, and R. W. Heath, "Modeling and analyzing millimeter wave cellular systems," *IEEE Trans. Commun.*, vol. 65, no. 1, pp. 403–430, Jan. 2017.
- [11] H. Wang, J. Fang, P. Wang, G. Yue, and H. Li, "Efficient beamforming training and channel estimation for millimeter wave OFDM systems," *IEEE Trans. Wireless Commun.*, vol. 20, no. 5, pp. 2805–2819, May 2021.
- [12] K. Venugopal, A. Alkhateeb, N. González Prelcic, and R. W. Heath, "Channel estimation for hybrid architecture-based wideband millimeter wave systems," *IEEE J. Sel. Areas Commun.*, vol. 35, no. 9, pp. 1996–2009, Sep. 2017.
- [13] J. Ma, S. Zhang, H. Li, F. Gao, and S. Jin, "Sparse Bayesian learning for the time-varying massive MIMO channels: Acquisition and tracking," *IEEE Trans. Commun.*, vol. 67, no. 3, pp. 1925–1938, Mar. 2019.
- [14] J. Ma, S. Zhang, H. Li, N. Zhao, and V. C. M. Leung, "Interference-alignment and soft-space-reuse based cooperative transmission for multi-cell massive MIMO networks," *IEEE Trans. Wireless Commun.*, vol. 17, no. 3, pp. 1907–1922, Mar. 2018.
- [15] X. Li, J. Fang, H. Duan, Z. Chen, and H. Li, "Fast beam alignment for millimeter wave communications: A sparse encoding and phaseless decoding approach," *IEEE Trans. Signal Process.*, vol. 67, no. 17, pp. 4402–4417, Sep. 2019.
- [16] M. Cheng, J. Wang, Y. Wu, X. Xia, K. Wong, and M. Lin, "Coverage analysis for millimeter wave cellular networks with imperfect beam alignment," *IEEE Trans. Veh. Technol.*, vol. 67, no. 9, pp. 8302–8314, Sep. 2018.
- [17] N. Bahadori, N. Namvar, B. Kelley, and A. Homaifar, "Device-to-device communications in millimeter wave band: Impact of beam alignment error," in *Proc. Wireless Telecommun. Symp.*, 2019, pp. 1–6.
- [18] M. Di Renzo, "Stochastic geometry modeling and analysis of multi-tier millimeter wave cellular networks," *IEEE Trans. Wireless Commun.*, vol. 14, no. 9, pp. 5038–5057, Sep. 2015.
- [19] C. Liu, M. Li, S. V. Hanly, I. B. Collings, and P. Whiting, "Millimeter wave beam alignment: Large deviations analysis and design insights," *IEEE J. Sel. Areas Commun.*, vol. 35, no. 7, pp. 1619–1631, Jul. 2017.
- [20] J. Zhang, Y. Huang, Q. Shi, J. Wang, and L. Yang, "Codebook design for beam alignment in millimeter wave communication systems," *IEEE Trans. Commun.*, vol. 65, no. 11, pp. 4980–4995, Nov. 2017.
- [21] M. Hussain, D. J. Love, and N. Michelusi, "Neyman-Pearson codebook design for beam alignment in millimeter-wave networks," in *Proc. ACM Workshop Millimeter-Wave Netw. Sens. Syst.*, 2017, pp. 17–22.
- [22] M. Hussain and N. Michelusi, "Energy-efficient interactive beam alignment for millimeter-wave networks," *IEEE Trans. Wireless Commun.*, vol. 18, no. 2, pp. 838–851, Feb. 2019.
- [23] C. Pradhan, A. Li, L. Zhuo, Y. Li, and B. Vucetic, "Beam misalignment aware hybrid transceiver design in mmWave MIMO systems," *IEEE Trans. Veh. Technol.*, vol. 68, no. 10, pp. 10306–10310, Oct. 2019.
- [24] C. Pradhan, A. Li, L. Zhuo, Y. Li, and B. Vucetic, "Hybrid-precoding for mmWave multi-user communications in the presence of beam-misalignment," *IEEE Trans. Wireless Commun.*, vol. 19, no. 9, pp. 6083–6099, Sep. 2020.
- [25] A. Thornburg and R. W. Heath, "Ergodic capacity in mmWave ad hoc network with imperfect beam alignment," in *Proc. IEEE Mil. Commun. Conf.*, 2015, pp. 1479–1484.

- [26] E. Turgut and M. C. Gursoy, "Coverage in heterogeneous downlink millimeter wave cellular networks," *IEEE Trans. Commun.*, vol. 65, no. 10, pp. 4463–4477, Oct. 2017.
- [27] M. S. Zia, D. M. Blough, and M. A. Weitnauer, "Coverage in millimeter-wave networks with SNR-dependent beam alignment errors," in *Proc. IEEE Veh. Technol. Conf.*, 2020, pp. 1–5.
- [28] J. Wildman, P. H. J. Nardelli, M. Latva-aho, and S. Weber, "On the joint impact of beamwidth and orientation error on throughput in directional wireless Poisson networks," *IEEE Trans. Wireless Commun.*, vol. 13, no. 12, pp. 7072–7085, Dec. 2014.
- [29] M. Haenggi, *Stochastic Geometry for Wireless Networks*. Cambridge, U.K.: Cambridge Univ. Press, 2012.
- [30] I. Ahmed *et al.*, "A survey on hybrid beamforming techniques in 5G: Architecture and system model perspectives," *IEEE Commun. Surveys Tuts.*, vol. 20, no. 4, pp. 3060–3097, Oct.–Dec. 2018.
- [31] M. Rihan, T. A. Soliman, C. Xu, L. Huang, and M. I. Dessouky, "Taxonomy and performance evaluation of hybrid beamforming for 5G and beyond systems," *IEEE Access*, vol. 8, pp. 74605–74626, 2020.
- [32] A. Alkhateeb, G. Leus, and R. W. Heath, "Limited feedback hybrid precoding for multi-user millimeter wave systems," *IEEE Trans. Wireless Commun.*, vol. 14, no. 11, pp. 6481–6494, Nov. 2015.
- [33] R. W. Heath, N. González-Prelcic, S. Rangan, W. Roh, and A. M. Sayeed, "An overview of signal processing techniques for millimeter wave MIMO systems," *IEEE J. Sel. Topics Signal Process.*, vol. 10, no. 3, pp. 436–453, Apr. 2016.
- [34] Y. Li, J. G. Andrews, F. Baccelli, T. D. Novlan, and C. J. Zhang, "Design and analysis of initial access in millimeter wave cellular networks," *IEEE Trans. Wireless Commun.*, vol. 16, no. 10, pp. 6409–6425, Oct. 2017.
- [35] A. Fascista, A. Coluccia, H. Wymeersch, and G. Seco-Granados, "Millimeter-wave downlink positioning with a single-antenna receiver," *IEEE Trans. Wireless Commun.*, vol. 18, no. 9, pp. 4479–4490, Sep. 2019.
- [36] M. Rebato, J. Park, P. Popovski, E. De Carvalho, and M. Zorzi, "Stochastic geometric coverage analysis in mmWave cellular networks with realistic channel and antenna radiation models," *IEEE Trans. Commun.*, vol. 67, no. 5, pp. 3736–3752, May 2019.
- [37] M. Shi, K. Yang, C. Xing, and R. Fan, "Decoupled heterogeneous networks with millimeter wave small cells," *IEEE Trans. Wireless Commun.*, vol. 17, no. 9, pp. 5871–5884, Sep. 2018.
- [38] A. F. Molisch *et al.*, "Millimeter-wave channels in urban environments," in *Proc. Eur. Conf. Antennas Propag.*, 2016, pp. 1–5.
- [39] O. E. Ayach, S. Rajagopal, S. Abu-Surra, Z. Pi, and R. W. Heath, "Spatially sparse precoding in millimeter wave MIMO systems," *IEEE Trans. Wireless Commun.*, vol. 13, no. 3, pp. 1499–1513, Mar. 2014.
- [40] C. Polprasert and J. A. Ritcey, "A Nakagami fading phase difference distribution and its impact on BER performance," *IEEE Trans. Wireless Commun.*, vol. 7, no. 7, pp. 2805–2813, Jul. 2008.
- [41] O. E. Ayach, R. W. Heath, S. Abu-Surra, S. Rajagopal, and Z. Pi, "The capacity optimality of beam steering in large millimeter wave MIMO systems," in *Proc. IEEE Int. Workshop Signal Process. Adv. Wireless Commun.*, 2012, pp. 100–104.
- [42] A. Alkhateeb, Y. Nam, M. S. Rahman, J. Zhang, and R. W. Heath, "Initial beam association in millimeter wave cellular systems: Analysis and design insights," *IEEE Trans. Wireless Commun.*, vol. 16, no. 5, pp. 2807–2821, May 2017.
- [43] 3GPP, "Technical specification group radio access network; study of radio frequency (RF) and electromagnetic compatibility (EMC) requirements for active antenna array system base station," 3GPP, Valbonne, France, Tech. Rep. TR 37.840, Dec., 2013.
- [44] C. A. Balanis, *Antenna Theory: Analysis and Design*. Hoboken, NJ, USA: Wiley, 2005.
- [45] H. L. Van Trees, *Optimum Array Processing: Part IV of Detection, Estimation, and Modulation Theory*. Hoboken, NJ, USA: Wiley, 2004.
- [46] S. Kusaladharma, W. Zhu, and W. Ajib, "Stochastic geometry-based modeling and analysis of massive MIMO-enabled millimeter wave cellular networks," *IEEE Trans. Commun.*, vol. 67, no. 1, pp. 288–301, Jan. 2019.
- [47] M. Abramowitz and I. A. Stegun, Eds., *Handbook of Mathematical Functions, With Formulas, Graphs, and Mathematical Tables*. Washington, DC, USA: NBS, 1964.
- [48] D. A. Fittipaldi and M. Luise, "Cramér-Rao bound for DOA estimation with antenna arrays and UWB-OFDM signals for PAN applications," in *Proc. IEEE Int. Symp. Pers., Indoor Mobile Radio Commun.*, 2008, pp. 1–5.
- [49] A. Gaber and A. Omar, "Utilization of multiple-antenna multicarrier systems and NLOS mitigation for accurate wireless indoor positioning," *IEEE Trans. Wireless Commun.*, vol. 15, no. 10, pp. 6570–6584, Oct. 2016.
- [50] H.-J. Kim, "Moments of truncated Student-*t* distribution," *J. Korean Statist. Soc.*, vol. 37, no. 1, pp. 81–87, Mar. 2008.
- [51] R. Li and S. Nadarajah, "A review of Student's *t* distribution and its generalizations," *Empirical Econ.*, vol. 58, no. 3, pp. 1461–1490, Mar. 2020.
- [52] S. Singh, F. Baccelli, and J. G. Andrews, "On association cells in random heterogeneous networks," *IEEE Wireless Commun. Lett.*, vol. 3, no. 1, pp. 70–73, Feb. 2014.
- [53] H. S. Dhillon and J. G. Andrews, "Downlink rate distribution in heterogeneous cellular networks under generalized cell selection," *IEEE Wireless Commun. Lett.*, vol. 3, no. 1, pp. 42–45, Feb. 2014.



Muhammad Saad Zia (Student Member, IEEE) received the B.E. and M.S. degrees in electrical engineering from the National University of Sciences and Technology, Pakistan, in 2012 and 2015, respectively. He is currently working toward the Ph.D. degree in electrical and computer engineering with the Georgia Institute of Technology, Atlanta, GA, USA. Before starting his Ph.D., he was an Assistant Director with the spectrum regulatory authority of Pakistan. His current research focuses on stochastic geometric analysis of millimeter-wave wireless networks.



Douglas M. Blough (Senior Member, IEEE) received the B.S. degree in electrical engineering, and the M.S. and Ph.D. degrees in computer science from Johns Hopkins University, Baltimore, MD, USA, in 1984, 1986, and 1988, respectively. He is currently a Professor of electrical and computer engineering with the Georgia Institute of Technology, Atlanta, GA, USA, where he also holds a joint appointment with the School of Computer Science. His research interests include wireless networks and dependable distributed systems. He has been on the Technical Program Committees of numerous conferences, including DSN, MobiHoc, MobiCom, MASS, Infocom, and ICDCS. He is on the Editorial Board of IEEE TRANSACTIONS ON WIRELESS COMMUNICATIONS and IEEE TRANSACTIONS ON CLOUD COMPUTING.



Mary Ann Weitnauer (Senior Member, IEEE) joined the School of Electrical and Computer Engineering, Georgia Tech, Atlanta, GA, USA, as an Assistant Professor in 1989 and is currently a Professor. She was a Visiting Professor with Aalborg University, Aalborg, Denmark, from 2006 to 2008 and with Idaho National Labs in 2010. From 2006 to 2012, she held the Georgia Tech ADVANCE Professorship with the College of Engineering. From 2016 to 2021, she was the Senior Associate Chair. She has authored or coauthored more than 200 refereed journal and conference papers. Her research focuses on the lower three layers of MIMO wireless networks that have virtual or distributed antenna arrays. Her team was the recipient of four best paper awards in conferences. From 2009 to 2012, she was an Associate Editor for IEEE TRANSACTIONS ON MOBILE COMPUTING.